R-phase shape memory alloy helical spring based actuators: Modeling and experiments

Pierre-Antoine Gédouin, Laurent Pino, Shabnam Arbab-Chirani, Sylvain Calloch, Emmanuel Delaleau, Jean-Matthieu Bourgeot

Submitted to *"Sensors and Actuators A: Physical"*, October 2018
Revised version, February 2019

R-phase Shape Memory Alloy Helical Spring Based Actuators: Modeling and Experiments

Pierre-Antoine Gédouin[a], Laurent Pino[b], Shabnam Arbab Chirani[b], Sylvain Calloch[c*],
Emmanuel Delaleau[a] and Jean-Matthieu Bourgeot[b]

[a] ENIB, F-29200 Brest, France

[b] ENIB, UMR CNRS 6027, IRDL, F-29200 Brest, France

[c] ENSTA Bretagne, UMR CNRS 6027, IRDL, F-29200 Brest, France

[*] Corresponding author. E-mail address: sylvain.calloch@ensta-bretagne.fr

Abstract

The main goal of this paper is to propose some analytical or pseudo-analytical tools facilitating the study and modeling of SMA helical spring-based actuators. Particular attention is paid to *R*-phase SMA helical spring-based actuators (*i.e.*, springs made in NiTi and concerned by *R*-phase transformation phenomena). First, simplified models (*i.e.,* based on beam theory framework) of *R*-phase SMA helical springs taking into account detwinning and assisted two-way memory effect are proposed and validated. Then, these models are used to determine the thermo-mechanical behavior of a linear bias-spring actuator. An actuator is built and used to validate the proposed models.

Keywords —NiTi, *R*-phase Transformation, SMA linear bias-spring actuator, simplified model.

1. Introduction

Shape Memory Alloys (*SMAs*) are one of the smart material families with a great potential for applications in some modern active structures, mainly as electrical or thermal actuators, e.g. [1-8]. Indeed, they have several characteristics that make them attractive for actuation applications: compact size, high power/weight ratio, high fatigue resistance to cyclic motion, and spark-free, clean and noiseless operation [9]. The interested reader can refer to the following references providing recent reviews focused on actuators triggered by shape memory alloys [10-12].

SMA based actuators generally work on Two-Way Memory Effect (*TWME*) and more precisely on Stress-Assisted Two-Way Memory Effect (*SATWME*). TWME is due to the spontaneous shape recovery induced during the low temperature martensitic phase and high temperature austenitic phase transformations. This unique and remarkable functional TWME is obtained typically after a special thermo-mechanical process called training [13]. When the shape memory material undergoes a thermal cycling at constant stress in place of the training procedure, it induces stress-assisted two-way memory effect in which martensitic transformation (or *R*-phase transformation) is assisted by the external stress, e.g. [14]. Figure 1 illustrates the SATWME schematically, where R_f^0, A_s^0, R_s^0 and A_f^0 are the four characteristic transformation temperatures under zero stress of the alloy. The thermo-mechanical loading is constituted by the two different stages (Fig. 1). The first stage (*i.e.*, path *AB*, Fig. 1) consists in applying a load at a constant temperature (*i.e.*, at low temperature $T_0 \leq R_f^0$) during which the reorientation process of thermal-induced martensite, M^T, (or thermal-induced *R*-phase, R^T) takes place. Then, the thermal-induced martensite, M^T, (or thermal-induced *R*-phase, R^T) is partially or totally replaced by stress-induced martensite, M^σ (or stress-induced *R*-phase, R^σ). After that, a thermal cycling under a constant stress level, τ_0, (*i.e.*, path *BCD*, Fig. 1) is applied during the second stage during which a macroscopic phase transformation strain occurs. The reverse phase transformation (*i.e.*,

$M^{\sigma} \rightarrow A$ or $R^{\sigma} \rightarrow A$) and the forward phase transformation (*i.e.*, $A \rightarrow M^{\sigma}$ or $A \rightarrow R^{\sigma}$) take place during the heating phase (*i.e.*, between *EF*, Fig. 1) and the cooling phase (*i.e.*, between *GH*, Fig. 1), respectively. The typical hysteretic transformation behavior of Shape Memory Alloys can be observed in the temperature-strain plane of Fig. 1.

The magnitude of SATWME depends heavily on the stress level and on the microstructural changes such as dislocations, reorientation of martensite variants and internal stress [14].

Thus, the large recoverable strain development occurring during SATWME is the basic principle in the operating of SMA based actuators. Therefore, generally, linear actuators using shape memory materials have a device to amplify the displacement either through the use of long straight wires [15-17] or through the use of helical springs [11, 18-20].

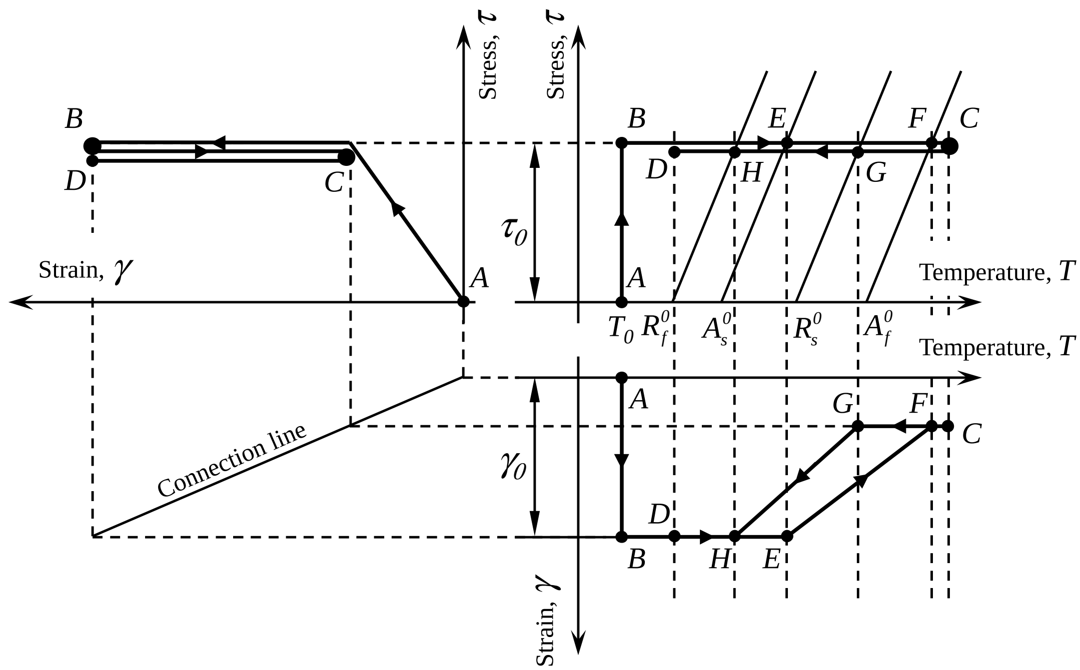

Fig. 1. Schematic representation of the stress-assisted two-way memory effect.

Description of the thermo-mechanical loading in the Temperature-Stress plane (T, τ).

Response of the material in the Temperature-Strain (T, γ) and the Strain-

Stress (γ, τ) planes.

Linear SMA helical spring-based actuators are more compact than SMA wire-based actuators. They generally create higher deflection and they have better fatigue performances. SMA-based actuators work under a constant or varying force to perform mechanical work. The actuator therefore generates force and motion upon heating or cooling. The simplest mode of operation is to work against a constant external force. As illustrated in Figure 2, a dead-weight is suspended from an SMA spring at low temperature. When the spring is heated above a certain temperature, its length changes. If the temperature returns to its initial value, the spring recovers its initial length. In the majority of applications, the dead-weight is replaced by a bias-spring (*i.e.*, a classic elastic spring) [11]. Consequently, the shape memory actuators work under varying forces and are activated by heat exchanges with the environment or by Joule effect.

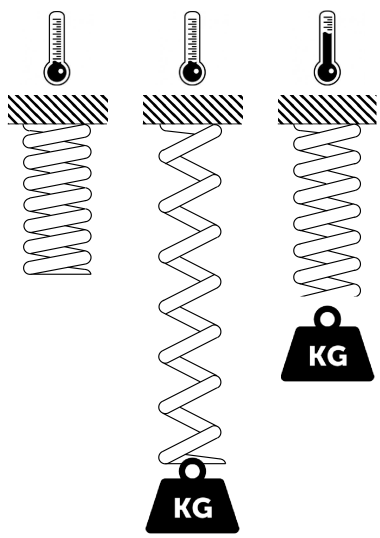

Fig. 2. Operating a simple SMA actuator consisting of an SMA helical spring
and a dead-weight.

Nevertheless, although a great number of patents and prototypes have been issued for Shape Memory Alloy (SMA) applications, few of them are commercially successful. This limited commercial success is due, on the one hand, to the complex and particular thermo-mechanical behavior of SMAs (*i.e.*, strongly non-linear) and on the other hand, to a lack of simple tools to aid the designers and developers of SMA applications. Therefore, the main goal of this paper is to propose some analytical or pseudo-analytical tools facilitating the study and modeling of linear SMA helical spring-based actuators. A particular attention is paid to *R*-phase SMA helical spring-based actuators (*i.e.*, springs made in NiTi and concerned by the *R*-phase transformation phenomena). Indeed, in the majority of NiTi alloys, another phase, called the *R*-phase, can occur in the material [21-23]. The *R*-phase appears before martensite from austenite during cooling. The recoverable strain due to this intermediate phase transformation is limited (*i.e.*, 0.25% to 0.75%) when compared with that of the martensite strain (*i.e.*, 6% to 10%, [13, 23]). A small hysteresis and a great stability of the thermo-mechanical behavior (*R*-phase ⇆ austenite) make this phase transformation interesting in the case of cyclic loading. This is why many commercial NiTi alloys for spring manufacturing have been developed to present *R*-phase transformation.

A large number of (thermo-)mechanical models of SMA helical springs have been proposed in the literature with the various degrees of sophistication. These (thermo-)mechanical models can be classified into two large families. The first is based on the use of the finite element method [24-32]. The second is based on beam theory and can be considered as a simplified approach [33-42]. In both cases, no model of SMA spring takes into account the specificities related to the *R*-phase.

The structure of this paper is as follows: first of all, simplified models adapted for *R*-phase NiTi based helical springs are proposed. The first is dedicated to the description of the reorientation process of the *R*-phase in a helical spring. The second concerns the description of the thermo-mechanical behavior of a stress-assisted two-way memory effect spring. These simplified models are based on beam theory framework in which well-adapted kinetics of phase transformations are considered. The two proposed models are validated using some experimental responses of NiTi springs. Then, a thermo-mechanical model of a linear bias-force actuator based on a serial association of an elastic helical spring with an *R*-phase SMA helical spring is proposed. A demonstrator is realized and used to validate the proposed model of bias-force actuator.

2. A simplified mechanical model for a pseudo-plastic SMA helical spring

2.1. Hypothesis

It is assumed that the material constituting all the considered springs is homogeneous and isotropic. The thermo-mechanical models proposed in the following have been developed according to the helical spring theory framework [43-44]. All helical springs, considered in this study, have a constant wire diameter, r, and a constant mean diameter of spring, D, with $R = ½ D$, the radius of spring. L_0 is the initial spring length and ϕ is the spring tilt angle (Fig. 3). Any external load, F, is applied along the spring axis. So, the external load and the dimensions of the helical spring imply that, locally, the spring wire is subjected to a pure shear loading [43-44].

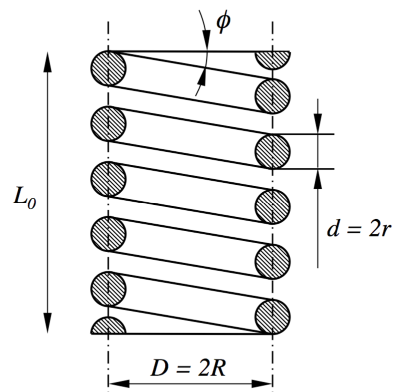

Fig. 3. Definition of the geometric parameters of the linear helical spring.

Let x be the radial distance between the center of the circular cross-section, O, and a point M of the cross-section (Fig. 4). The local shear strain, $\gamma(M)$, is expressed as:

$$\gamma(M) = \theta \cdot x \text{ with } 0 \leq x \leq r \tag{1}$$

where θ is the unitary torsion angle.

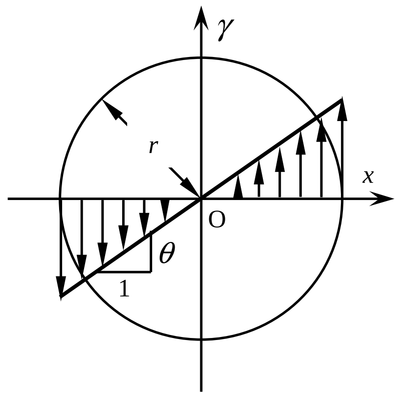

Fig. 4. Shear strain distribution in the wire cross-section of the helical spring.

The spring deflection, *f*, can be expressed as:

$$f = L - L_0 = 2\pi n \theta R^2 \qquad (2)$$

where *L* is the spring length subjected to a loading *F* and *n* is the number of coils. The principle of static equilibrium of moments applied to a helical spring section gives the relationship between the external load, F, and the torque, M_t, subjected by the cross-section:

$$M_t = F\frac{D}{2} = \int_S \tau(M) \cdot x \, dS \qquad (4)$$

At this stage, all the necessary elements to develop detwinning and stress-assisted two-way memory helical spring thermo-mechanical simplified models are available.

2.2. Mechanical behavior of an R-phase pseudo-plastic SMA

R-phase pseudo-plasticity, also called *R*-phase detwinning, concerns the isothermal mechanical behavior of thermal-induced *R*-phase, R^T. Under mechanical loading, the reorientation process of R^T takes place, giving rise to stress-induced R-phase, R^σ, and to a macroscopic strain. After unloading, a residual strain (*i.e.*, permanent strain) remains which can disappear after a heating; it is the memory effect. The pseudo-plastic behavior is not directly used in the SMA actuators, but it is very important in the actuator pre-straining stage (*i.e.*, assembly step). That is why a simplified model of mechanical behavior of an *R*-phase pseudo-plastic SMA helical spring taking into account the peculiarities of the mechanical behavior of thermal-induced *R*-phase, R^T, is proposed hereafter.

Figure 5 shows the schematic detwinning behavior of the thermal-induced *R*-phase, R^T, under a pure shear loading, τ.

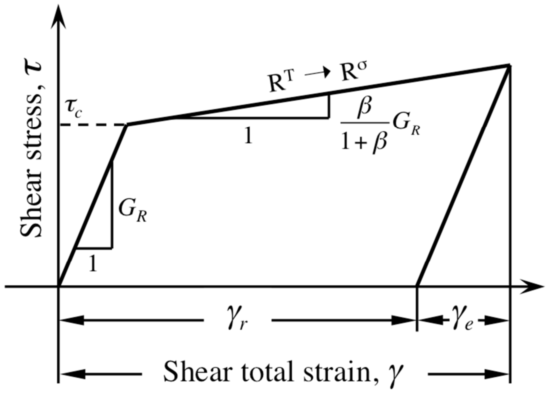

Fig. 5. Schematic detwinning behavior of the thermal-induced *R*-phase under pure shear loading.

Let τ_c represent the yield reorientation shear stress. Thus, until $\tau \leq \tau_c$, the mechanical behavior is purely elastic:

$$\tau = G_R \cdot \gamma = G_R \cdot \gamma_e \tag{5}$$

where G_R is the shear modulus of the thermal-induced *R*-phase, γ and γ_e are the total and the elastic shear strain, respectively.

Once $\tau > \tau_c$, the reorientation process of thermal-induced *R*-phase takes place, giving rise to a reorientation strain, γ_r, defined by:

$$\gamma = \gamma_e + \gamma_r = \frac{\tau}{G_R} + \gamma_r \tag{6}$$

Considering the schematic detwinning behavior of the thermal-induced *R*-phase (Fig. 5), a linear "pseudo-hardening" is assumed to take into account the evolution of the reorientation yield stress with the reorientation strain:

$$\gamma = \gamma_e + \gamma_r = \underbrace{\frac{\tau}{G_R}}_{\gamma_e} + \underbrace{\frac{(\tau - \tau_c)}{\beta G_R}}_{\gamma_r} \quad \Rightarrow \quad \tau = \frac{\beta G_R}{1+\beta}\gamma + \frac{\tau_c}{1+\beta} \tag{7}$$

where β is a material parameter and (βG_R) represents the pseudo-hardening modulus under pure shear loading.

Consequently, the constitutive equations of the mechanical behavior of the thermal-induced *R*-phase, under monotonic pure shear loading, can be summarized as follows:

$$\begin{cases} \tau = G_R \gamma_e = G_R \gamma & \text{for} \quad \tau \le \tau_c \\ \tau = \dfrac{\tau_c}{1+\beta} + \dfrac{\beta}{1+\beta} G_R \gamma & \text{for} \quad \tau > \tau_c \end{cases} \tag{8}$$

2.3. Mechanical behavior of a pseudo-plastic SMA helical spring

The constitutive material model, given by Eqn. (8), can be introduced in the mechanical behavior of the *R*-phase pseudo-plastic SMA helical spring. Figures 6a-c show shear strain and shear stress distributions in the spring cross-section.

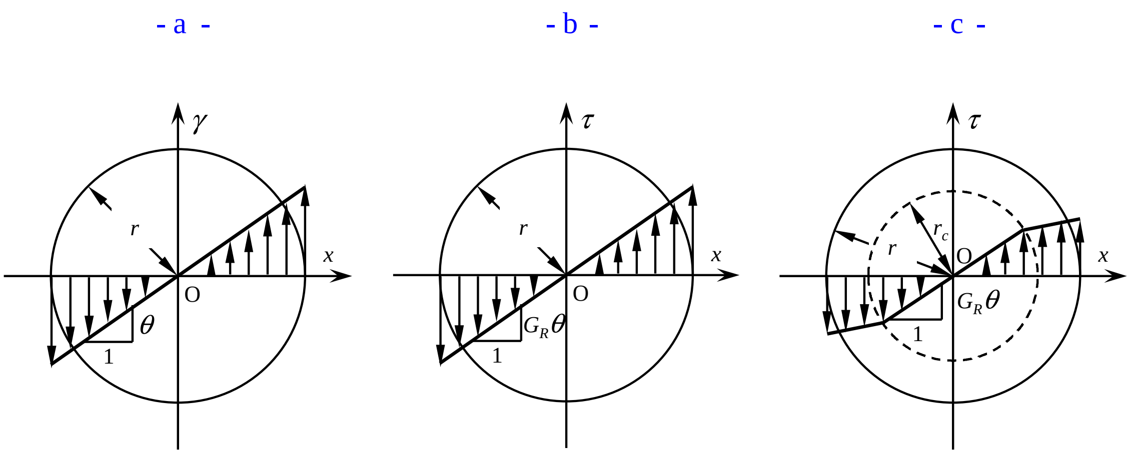

Fig. 6. Shear strain and stress distributions in the wire cross-section of the helical spring:

- a - shear strain distribution, ($\gamma(x) = \theta \cdot x$)

- b - shear stress distribution for $\tau(r) \le \tau_c$ (*i.e.*, elastic case)

- c - shear stress distribution for $\tau(r) > \tau_c$ (*i.e.*, pseudo-plastic case)

Thus, the relation between the torque subjected by the cross-section, M_t, and the unitary torsion angle, θ, is given by the equilibrium moment equation of the wire cross-section of the helical spring:

$$\begin{cases} M_t = F\dfrac{D}{2} = \int_S \tau(x)\cdot x\cdot 2\pi x\,dx = 2\pi\int_0^r G_R\,\theta x^3\,dx & \text{if} \quad F \le \dfrac{\tau_c\pi r^3}{D} \\ M_t = F\dfrac{D}{2} = \int_S \tau(x)\cdot x\cdot 2\pi x\,dx = 2\pi\int_0^{r_c} G_R\,\theta x^3\,dx + 2\pi\int_{r_c}^r \dfrac{\tau_c+\beta G_R\,\theta x}{1+\beta}x^2dx & \text{if} \quad F > \dfrac{\tau_c\pi r^3}{D} \end{cases} \tag{9}$$

In the last relation, r_c is the radius where the shear stress reaches the yield reorientation shear stress, τ_c:

$$\tau_c = G_R\cdot\gamma(x=r_c) = G_R\cdot\theta\cdot r_c \qquad \Rightarrow \qquad r_c = \frac{\tau_c}{G_R\cdot\theta} \tag{10}$$

Finally, the torque subjected by the cross-section, M_t, is given by the following relation:

$$\begin{cases} M_t = F\dfrac{D}{2} = \pi G_R\,\theta\dfrac{r^4}{2} & \text{if} \quad F \le \dfrac{\tau_c\pi r^3}{D} \\ M_t = F\dfrac{D}{2} = \pi G_R\,\theta\dfrac{r_c^4}{2} + \dfrac{2\pi}{3}\tau_c\left(r^3-r_c^3\right) + 2\pi\dfrac{\beta}{1+\beta}G_R\,\theta\left(\dfrac{r^4}{4}-\dfrac{r_c r^3}{3}+\dfrac{r_c^4}{12}\right) & \text{if} \quad F > \dfrac{\tau_c\pi r^3}{D} \end{cases} \tag{11}$$

Finally, by considering Eqns. (2), (10) and (11), one can find the relation between the external load, F, and the spring deflection, f:

$$\begin{cases} F = \dfrac{G_R\,d^4}{8nD^3}f & \text{if} \quad F \le \dfrac{\tau_c\pi r^3}{D} \\ F = \dfrac{\pi\tau_c d^3}{6D}\left(\dfrac{1}{1+\beta}\right)\left(1-\dfrac{1}{4}\left(\dfrac{n\pi\tau_c D^2}{dG_R\,f}\right)^3\right) + \dfrac{\beta}{1+\beta}\dfrac{G_R\,d^4}{8nD^3}f & \text{if} \quad F > \dfrac{\tau_c\pi r^3}{D} \end{cases} \tag{12}$$

Equation (12) represents an analytical expression of the mechanical behavior of an *R*-phase pseudo-plastic SMA helical spring. This type of model (*i.e.*, analytical model) gives, in a simple way, the influence of the six geometric and material parameters (*i.e.*, D, d, n, G_R, τ_c and β) on the mechanical response of the spring. Figure 7 shows the evolution of the external load, F, as a function of the helical spring deflection, f.

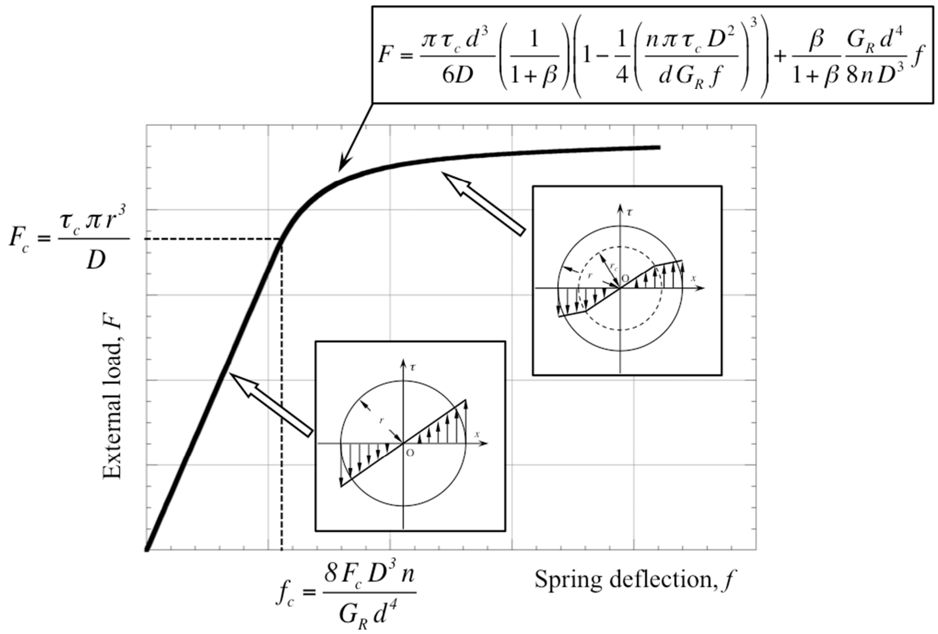

Fig. 7. Mechanical behavior of an R-phase pseudo plastic SMA helical spring.

External load, F, versus spring deflection, f.

(Values of the six parameters: D = 6,3 mm, d = 0,75 mm, n = 24, G_R = 20 000 MPa, τ_c = 26,6 MPa and β = 0,01)

2.4. *Identification of the simplified pseudo-plastic SMA helical spring model*

This section is devoted to the description and the realization of mechanical tests on an SMA helical spring. The experimental results were used to identify the simplified mechanical model presented in the previous section.

An experimental apparatus, comprising an electromechanical testing machine with a thermal chamber of up to 300°C, was employed to investigate the thermomechanical behavior of SMA helical springs. The set up had a 50 N load cell and a very sensitive displacement sensor (*i.e.*, 5 µm resolution). An SMA NiTi (*i.e.*, Nickel Titanium) helical spring with a diameter, D, of 6.3 mm, a wire diameter of 0.75 mm and 24 active coils was used. The characteristic transformation temperatures of our NiTi alloy were determined using DSC analysis. The four transformation temperatures, R_f^0, R_s^0, A_s^0 and A_f^0, are given in Table 1. Our SMA NiTi helical spring was in an R-phase state at room temperature. Finally, the SMA spring was directly connected to the machine's jaws (Fig. 8).

Then, a simple tensile test under displacement control at room temperature (*i.e.*, 22°C), in quasi-static conditions, was performed. Figure 9 shows the deflection/force response curve of the helical spring. Between points A and B, the spring behavior was elastic and between points B and C, *R*-phase detwinning took place. The comparison between experimental results and the simplified mechanical model proposed is also shown in Fig. 9. The three material parameters, G_R, τ_c and β (Eqn. (12)), have been identified by minimization, in a least-squares sense, of the distance between model response and experimental data. Table 2 gives the numerical values of the six parameters of the simplified *R*-phase pseudo-plastic SMA helical spring model proposed.

R-phase finish temperature, R_f^0	*R*-phase start temperature, R_s^0	Austenite start temperature, A_s^0	Austenite finish temperature, A_f^0
35 °C	45 °C	39 °C	51,5 °C

Tab. 1. The characteristic transformation temperatures of the NiTi spring.

D (mm)	d (mm)	n	G_R (MPa)	τ_c (MPa)	β
6.3	0.75	24	20000	27	3.2

Tab. 2. The six identified parameters of the simplified pseudo-plastic SMA spring model.

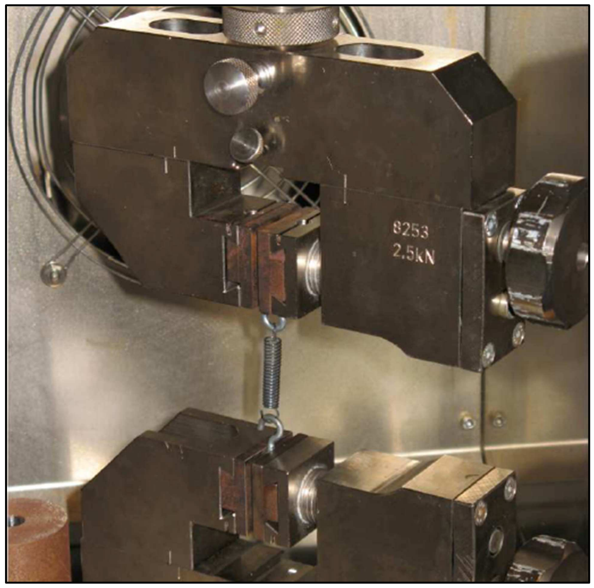

Fig. 8. Experimental set up for detwinning tensile test on the NiTi SMA helical spring.

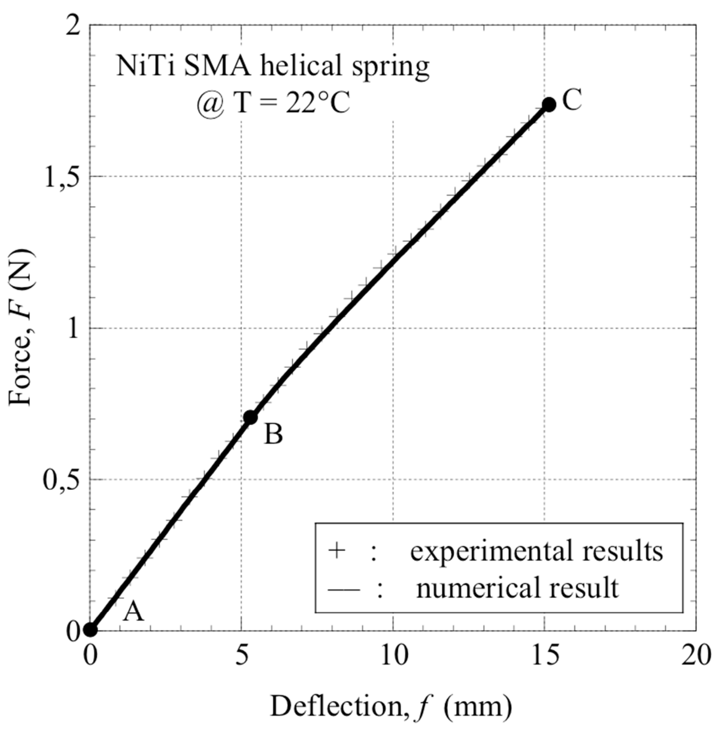

Fig. 9. Deflection/force response curves of the NiTi SMA helical spring at room temperature.

3. A simplified thermo-mechanical model for a stress-assisted two-way SMA helical spring

3.1. Hypothesis

In this section, a simplified model of the thermo-mechanical behavior of a stress-assisted two-way *R*-phase SMA spring taking into account the peculiarities of the SATWME of *R*-phase is proposed.

Thus, the main goal is to propose a thermo-mechanical model able to describe the behavior of an *R*-phase SMA spring subjected to a thermal loading under constant load (Fig. 2). As previously mentioned, particular attention is paid to the SATWME of the *R*-phase and to cyclic thermal loadings.

The hypothesis and the notations used in this section are the same as those considered in the previous section (*i.e.*, § 2).

3.2. Thermo-mechanical behavior of a stress-assisted two-way SMA

Classically, there are two different ways to obtain the SATWME. The first, as explained in the introduction (Fig. 1), is realized by first applying an isothermal mechanical loading in the thermal-induced *R*-phase state, R^T, until a stress level higher than reorientation yield stress (path AB, Fig. 1). This applied stress is maintained at a constant and then a thermal cycling is performed (path BCD, Fig. 1). During this thermal cycle, the stress-induced *R*-phase, R^σ, transforms into the austenite phase. The second solution is obtained by first applying an isothermal mechanical loading in the austenite phase state ($T > A_f^0$) (path A'B', Fig. 10). This applied stress is maintained at a constant and then a thermal cycling is performed (path B'C'B', Fig. 10). During this thermal cycle, the austenite phase transforms into the stress-induced *R*-phase, R^σ. In both cases, a recoverable strain up to 0.75% can be generated, and that is directly used in the functioning of the *R*-phase Shape Memory Alloy helical spring based actuators.

Before proposing a thermo-mechanical model describing the behavior of a stress-assisted two-way *R*-phase SMA spring, constitutive equations for assisted two-way memory effect are proposed.

In a small perturbation framework, the following shear strain decomposition is assumed:

$$\gamma = \gamma^{e} + \gamma^{tr} + \gamma^{cd} \tag{13}$$

where γ^{e} is the elastic shear strain related to the shear stress, τ, represented by the following equation:

$$\gamma^{e} = \frac{\tau}{G} \tag{14}$$

where G is the shear modulus of the material given by:

$$G = G_A\left(1 - z\right) + G_R\, z \tag{15}$$

where G_A and G_R are the shear modulus of the austenite and the R-phase, respectively, and z is the volume fraction of the stress-induced R-phase. γ^{tr} is the shear strain due to the phase transformation between the austenite and stress-induced R-phase and γ^{cd} is the shear strain associated to a special deformation mechanism of the R-phase called R-phase continuous distortion [21-22]. According to the experimental results of Šittner and his colleagues [21-22], the R-phase continuous distortion shear strain can be written as:

$$\gamma^{cd} = -a \cdot \left(T - T_{ref}\right) \cdot z \tag{16}$$

where T is the temperature and a a material parameter. Eqn. (16) can be justified by two experimental observations. First, there is no continuous distortion without R-phase (*i.e.*, $z = 0$). Second, when there is no austenite, the continuous distortion strain is a linear decreasing function of the temperature rise, $\left(T - T_{ref}\right)$.

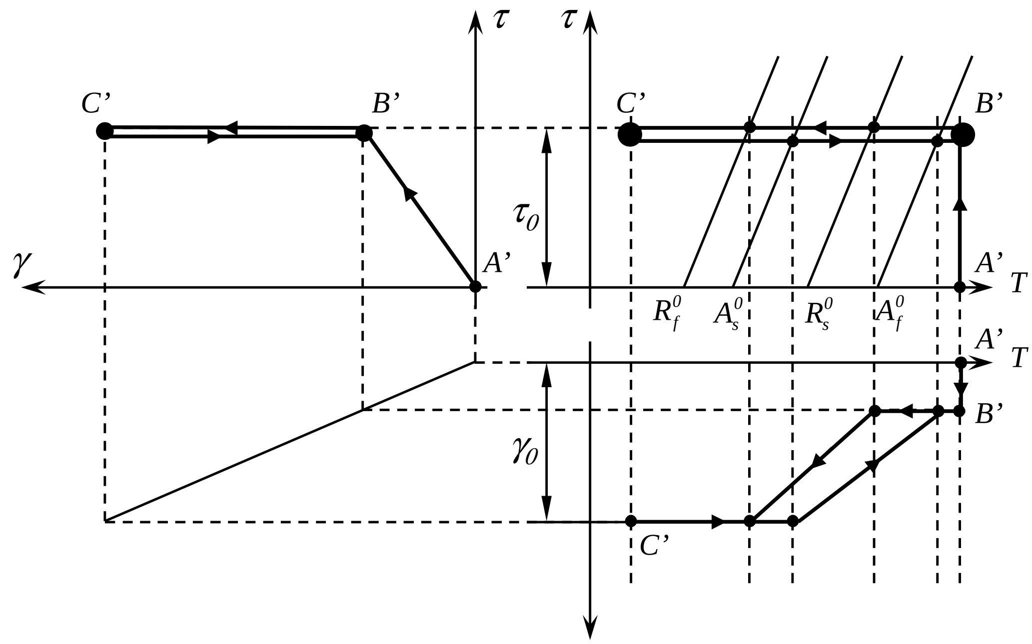

Fig. 10. Schematic representation of the stress-assisted two-way memory effect.

Description of the thermo-mechanical loading in the Temperature-Stress plane (T, τ).

Response of the material in the Temperature-Strain (T, γ) and the Strain-Stress (γ, τ) planes.

A linear relation between the transformation strain and the volume fraction of stress-induced *R*-phase has been experimentally validated by Taillard *et al.* [45]:

$$\gamma^{tr} = \mu^{tr} z \tag{17}$$

where μ^{tr} is the maximum transformation shear strain of the material. Eqns. (13), (14), (15), (16) and (17) give:

$$\gamma = \frac{\tau}{G_A(1-z) + G_R z} + \left(\mu^{tr} - a \cdot \left(T - T_{ref}\right)\right) \cdot z \tag{18}$$

Thus, the last step is to define the transformation kinetics describing the evolution of the volume fraction of stress-induced *R*-phase, *z*, during the thermo-mechanical loading. We assume that the stress level, τ_0 (Fig. 10), is smaller than the yield stress of the austenite (*i.e.*, onset transformation stress) and high enough to induce maximal transformation strain during the thermal loading (*i.e.*, path B'C'B', Fig. 10). In these conditions, the volume fraction of the stress-induced *R*-phase depends only on the temperature, *T*, on the sign of the temperature variation, $sign(\dot{T})$, on the stress level, τ, and on two memory variables, *v* and *w*, defined in the following. The variables, *v* and *w* will enable the internal hysteresis loops to be managed simply.

The envelope of the response of the material, denoted as z_e, can be modeled by means of two branches. The first corresponds to the heating phase and the second to the cooling phase:

$$z_e(T,\tau)=\begin{cases}\psi_1(T,\tau)+1 & \text{if} \quad \dot{T}>0\\ \psi_2(T,\tau) & \text{if} \quad \dot{T}\leq 0\end{cases} \tag{19}$$

where ψ_1 and ψ_2 are two shape functions defined as follows:

$$\begin{cases}\psi_1(T,\tau)=-\dfrac{1}{2}\Big[1+sign\big(T-A(\tau)\big)\times\big(1\text{-}exp\big(-C\left|T-A(\tau)\right|\big)\big)\Big]\\ \psi_2(T,\tau)=\dfrac{1}{2}\Big[1\text{-}sign\big(T-R(\tau)\big)\times\big(1\text{-}exp\big(-C\left|T-R(\tau)\right|\big)\big)\Big]\end{cases} \tag{20}$$

with:

$$\begin{cases}A(\tau)=\dfrac{A_s^0+A_f^0}{2}+\lambda\cdot\tau\\ R(\tau)=\dfrac{R_s^0+R_f^0}{2}+\lambda\cdot\tau\end{cases} \tag{21}$$

In Equations (18) and (19), *C* and λ are two material parameters and A_s^0, A_f^0, R_s^0 and R_f^0 are the characteristic temperatures of the phase transformation at zero stress (Fig. 10). The evolution of the transformation temperatures according to the shear stress level is given by Eqn. (19). This enables the hysteresis loop to move to a higher temperature when the shear stress level increases. Internal loops, confined in the envelope z_e, are described by the following equations:

$$\dot{T} > 0, \quad \begin{cases} z = w \cdot \psi_1(T,\tau) + w \\ \dot{w} = 0 \\ v = \dfrac{\left(z - \psi_2(T,\tau)\right)}{\left(1 - \psi_2(T,\tau)\right)} \end{cases} \tag{22}$$

$$\dot{T} \leq 0, \quad \begin{cases} z = (1-v) \cdot \psi_2(T,\tau) + v \\ w = \dfrac{z}{\left(1 + \psi_1(T,\tau)\right)} \\ \dot{v} = 0 \end{cases} \tag{23}$$

where v and w are initialized between 0 and 1. For example, if $w = 1$ and $\dot{T} > 0$, initially, then z is on the increasing temperature branch of envelope z_e (Eqn. (22)). In the same way, if $v = 0$ and $\dot{T} \leq 0$, initially, then z is on the decreasing temperature branch of the envelope z_e (Eqn. (23)). Moreover, it is important to note that the expression of the two shape functions, $\psi_1(T,\tau)$ and $\psi_2(T,\tau)$, depend on the material behavior (*i.e.*, the hysteresis shape).

An example of the evolution of the volume fraction of the stress-induced *R*-phase as a function of temperature at constant stress is given in Figure 11.

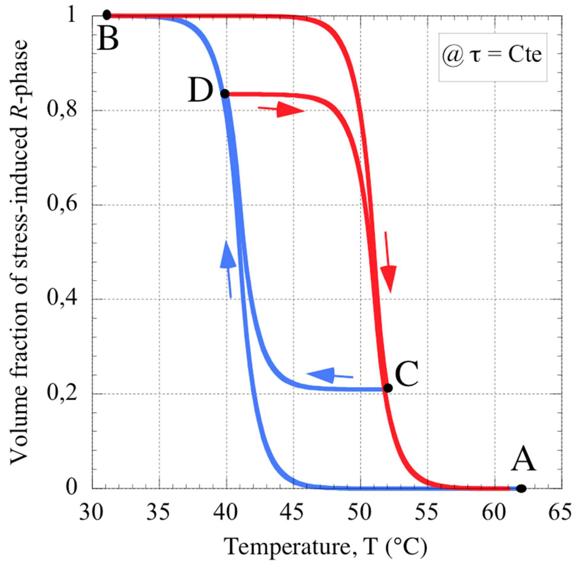

Fig. 11. Example of evolution of the volume fraction of the stress-induced *R*-phase, *z*, during a thermal loading "A-B-C-D-A" at constant stress.

3.3. Thermo-mechanical behavior of a stress-assisted two-way SMA spring

This kinetics of phase transformation, proposed previously, is now integrated in a thermo-mechanical model describing the behavior of a stress-assisted two-way *R*-phase SMA helical spring (*i.e.*, the relation between deflection, temperature and external force).

Set τ_s and z_s, the shear stress and the volume fraction of *R*-phase on the skin of the wire cross-section of the helical spring, respectively. Eqn. (1) gives the shear strain at the skin of the wire cross-section of the spring, γ_s:

$$\gamma_s = \theta \frac{d}{2} \tag{24}$$

Using Eqns. (2), (18) and (24) at the skin of the wire cross-section of the spring, gives:

$$f = \frac{\pi n D^2}{d} \left(\frac{\tau_s}{G_a (1 - z_s) + G_R z_s} + \left(\mu^{tr} - a \cdot \left(T - T_{ref} \right) \right) \cdot z_s \right) \tag{25}$$

where τ_s, constant during transformation, is given by:

$$\tau_s = \frac{8FD}{\pi \mathrm{d}^3} \tag{26}$$

Using the two last equations, one obtains:

$$f = \frac{F}{K_a(1-z_s)+K_R z_s} + \frac{\pi n D^2}{d}\left(\mu^{tr} - a.\left(T - T_{ref}\right)\right).z_s \tag{27}$$

where $K_a = \dfrac{G_a d^4}{8nD^3}$ and $K_R = \dfrac{G_R d^4}{8nD^3}$ are the helical spring stiffness in the austenitic and *R*-phase state, respectively. In Eqn. (27), z_s, the volume fraction of the *R*-phase at the skin of the wire cross-section of the helical spring, depends on the temperature, *T*, and the shear stress, τ_s and is given by the equations of phase transformation kinetics, Eqns (19) (22) and (23). Thus, Eqn. (27) gives the evolution of the deflection of a stress-assisted two-way *R*-phase SMA helical spring under a constant external load and during a thermal loading.

3.4. Identification and validation of the simplified stress-assisted two-way SMA helical spring model

This section is devoted to the description and realization of a series of Stress-Assisted Two-Way tests on an *R*-phase SMA helical spring. The SMA springs used in this part are the same as those used in §2.4.

The first SATW tests had two stages: first, an initial isothermal mechanical loading was applied at high temperature (*i.e.*, T = 55°C > A_f^0). In this stage, the helical spring was in an austenitic state and remained elastic. Then, a cooling/heating cycle was applied between 55°C and 26°C with a cooling and heating rate of ±1°C/min. Five different levels of external force were considered (*i.e.*, 0.7, 1, 1.3, 1.5 and 1.7 N). The tests at 0.7 and 1.3 N were used to identify the simplified stress-assisted two-way *R*-phase SMA helical spring model presented in the previous section and the others were used in the validation stage of the proposed model.

Figure 12 shows the evolution of the *R*-phase SMA helical spring deflection, *f*, versus temperature, *T*, for two SATW tests performed at 0.7 and 1.3 N, respectively. The SATW test, performed at 0.7 N, consists in a cooling between 54°C to 26°C, while the test performed at 1.3 N is a thermal cycle between 55°C and 26°C (Fig. 12).

The seven material parameters of the proposed thermo-mechanical model of stress-assisted two-way *R*-phase SMA spring (*i.e.*, G_a, μ^{tr}, a, C, $A_0 = \frac{1}{2}\left(A_s^0 + A_f^0\right)$, $R_0 = \frac{1}{2}\left(R_s^0 + R_f^0\right)$ and λ) were identified using the two experimental results given in Fig. 12. Table 3 gives the set of numerical values of the parameters of the simplified thermo-mechanical model of stress-assisted two-way *R*-phase SMA spring. Figure 13 shows the comparison between experimental and numerical results for the SATW tests performed at 1.0, 1.3, 1.5 and 1.7 N, respectively. One can observe a good agreement between the numerical results and experimental data.

Finally, another type of SATW test was carried out under complex temperature history (*i.e.*, the thermal loading includes an internal cycle) at a constant external force of 1.2 N. Figure 14 shows the thermal loading. Figure 15 shows the comparison between experimental and numerical results. Again, there is a good agreement between the numerical results and experimental data.

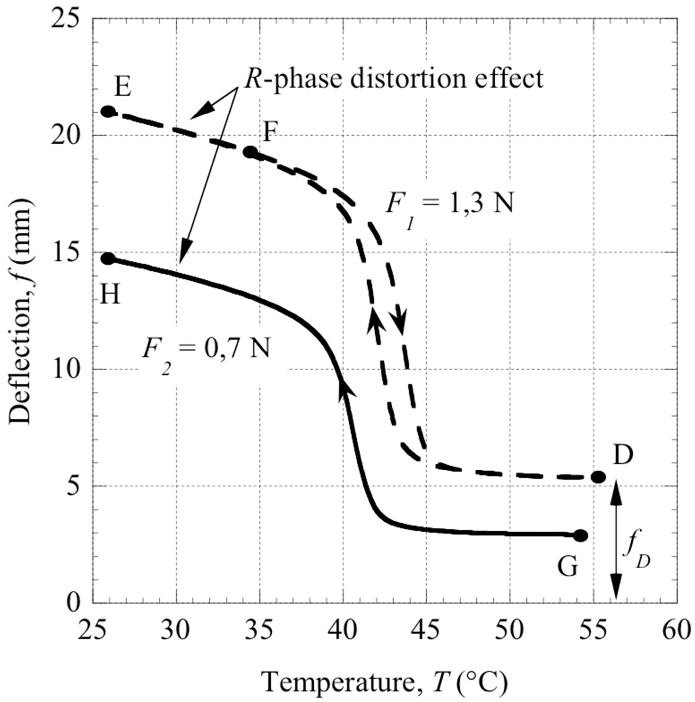

Fig. 12. Evolution of deflection versus temperature for two stress-assisted two-way tests on an *R*-phase SMA helical spring.

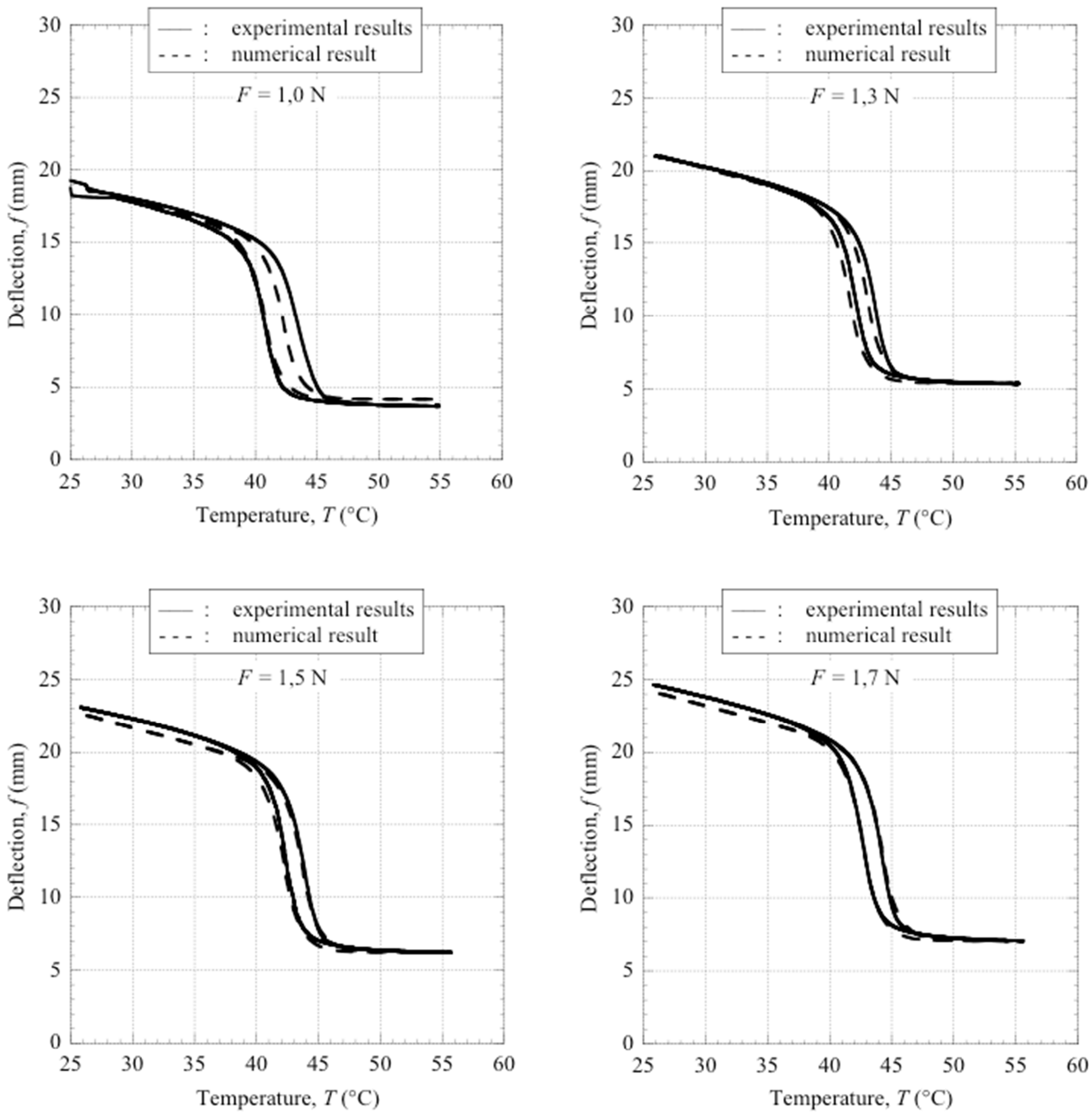

Fig. 13. Stress-assisted two-way tests at different constant efforts: comparison between experimental and numerical results.

G_R (MPa)	G_a (MPa)	μ^{tr} (%)	a (°C^{-1})
20000	36500	0.43	5.77×10^{-3}
C (°C^{-1})	**A_0 (°C)**	**R_0 (°C)**	**λ (°C.MPa^{-1})**
0.87	59.5	38	3.25×10^{-2}

Tab. 3. The identified parameters of the simplified stress-assisted two-way *R*-phase SMA spring model.

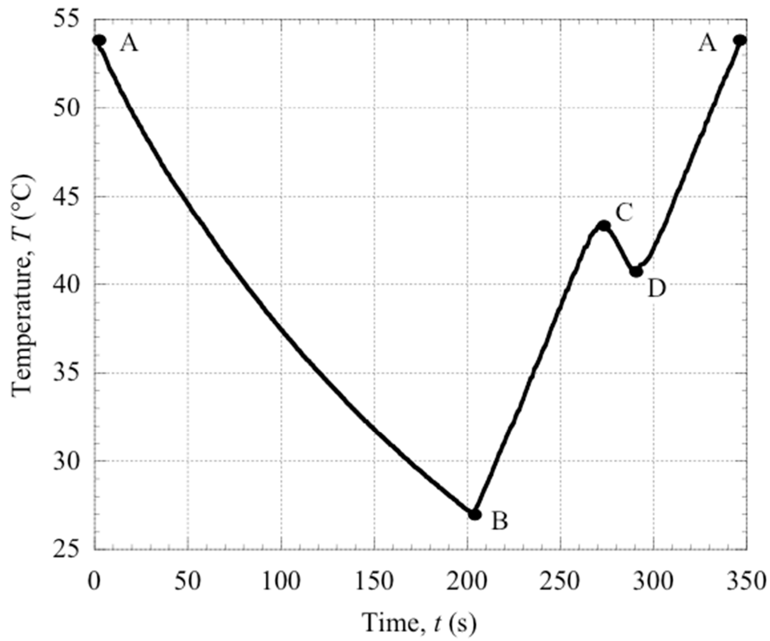

Fig. 14. Description of the complex thermal loading with internal cycle.

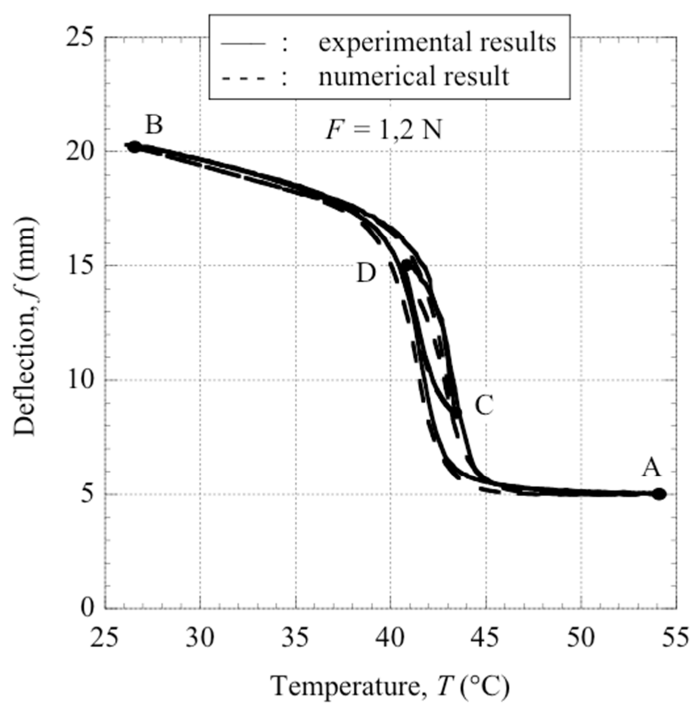

Fig. 15. Comparison between experimental and numerical results for the complex thermal loading with internal cycle.

4. A simplified thermo-mechanical model for linear bias-spring actuators

4.1. Hypothesis

This last section concerns the modeling of the thermo-mechanical behavior of linear bias-spring actuators. Linear bias-spring actuators are an important category of SMA-based actuators. They are typically used in contexts that require multiple cyclic operations or actuations. Since SMA linear actuators can only contract in one direction, a biasing force is necessary to return the SMA to its neutral position. The biasing force is classically generated by a preload spring (*i.e.*, bias-elastic spring). Figure 16 shows the typical architecture of a linear bias-spring actuator associating an SMA spring with a bias-elastic spring in a differential arrangement.

Fig. 16. Typical SMA linear bias-elastic spring actuator design.

In the following, a simplified thermo-mechanical model for linear bias-spring actuators is proposed in a quasi-static framework (*i.e.*, the inertia effects are ignored). Particular attention is paid to linear bias-spring actuators based on the use of a stress-assisted two-way *R*-phase SMA helical spring. Thus, the proposed model is based on the use of the simplified model developed and described in the previous sections.

4.2. Thermo-mechanical behavior of linear bias-elastic spring actuators

Figure 17 shows the two stages that have to be considered in the modeling of the thermo-mechanical behavior of an SMA linear bias-elastic spring actuator. The first, called *prestrain stage* or *mounting stage*, is performed at low temperature (*i.e.*, a temperature lower than the *R*-phase finish temperature, R_f^0). At this stage, the *R*-phase SMA spring is in a thermal-induced *R*-phase state and is mechanically loaded to connect it with the bias-elastic spring. After this step, the mobile part of the

actuator, initially located in position *A*, moves to position *B* (Fig. 17). The *R*-phase SMA spring is thus subjected to a detwinning loading. Therefore, to model this first stage, the detwinning model, proposed in § 2, is used.
The second stage concerns the actuation of the SMA linear bias-elastic spring actuator (Fig. 17). The *R*-phase SMA spring is alternately heated and cooled. During the first heating, the mobile part moves from position *B* to position *C*, depending on the temperature level and preloading (Fig. 17). Then, during the next thermal cycles, the mobile part evolves between the two positions *C* and *D* (Fig. 17). To model this second stage, the simplified thermo-mechanical model for a stress-assisted two-way *R*-phase SMA helical spring, proposed in §3, is used.

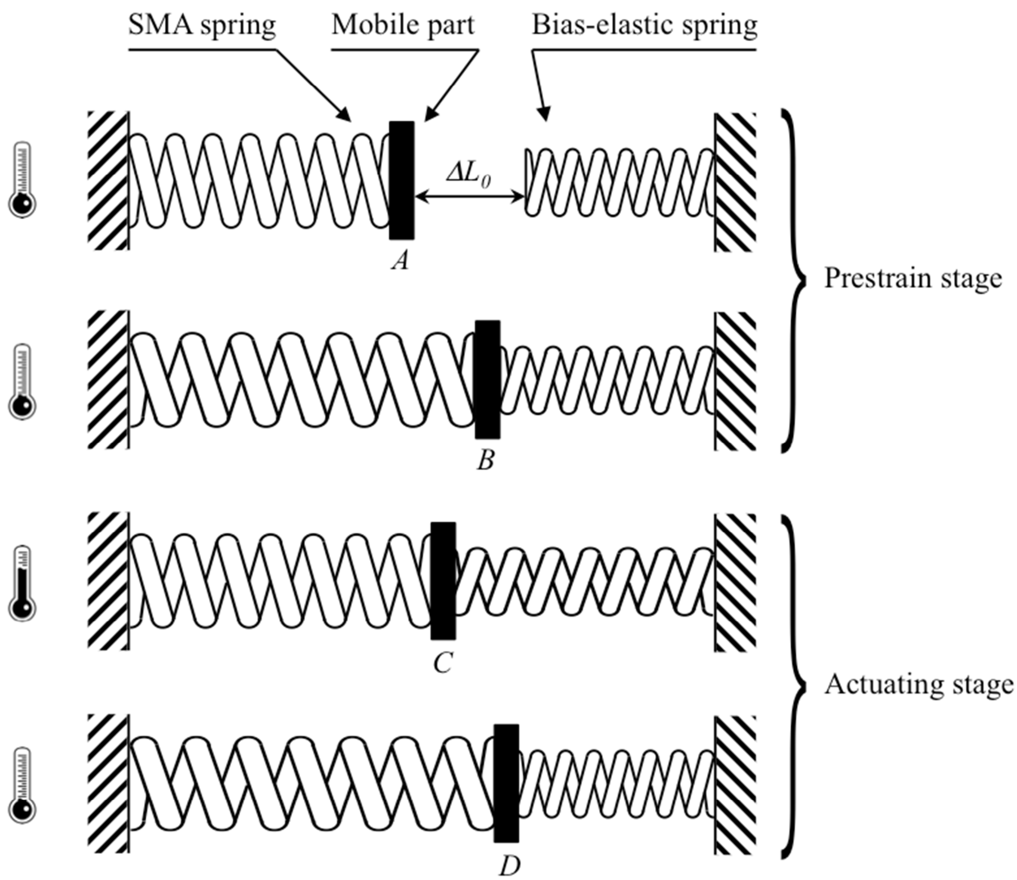

Fig. 17. Schematic representation of the two stages in the operation of an SMA linear bias-elastic spring actuator.

In the following, a mechanical modeling of the two stages described above is proposed. The prestrain phase is first processed followed by the actuating stage.

During the prestrain stage, it is assumed that the force generated by the bias-elastic spring is not sufficient to induce the martensite transformation in the SMA spring. Only the reorientation process of the *R*-phase is taken into account. The four quantities, f_B^e (*i.e.*, the initial deflection of the elastic spring), f_B^{SMA} (*i.e.*, the initial deflection of the SMA spring), F_B^e (*i.e.*, the force exerted by the elastic spring on the mobile part) and F_B^{SMA} (*i.e.*, the force exerted by the SMA spring on the mobile part), define the state of the SMA actuator in position *B*. They can be determined using the four following equations:

Mechanical behavior of elastic spring: $F_B^e = K^e f_B^e$ (28)

Mechanical behavior of SMA spring (Eq. (12)):

$$F_B^{SMA} = \frac{\pi \tau_c d^3}{6D} \left(\frac{1}{1+\beta} \right) \left(1 - \frac{1}{4} \left(\frac{n \pi \tau_c D^2}{d G_R f_B^{SMA}} \right)^3 \right) + \frac{\beta}{1+\beta} \frac{G_R d^4}{8 n D^3} f_B^{SMA} \tag{29}$$

Equilibrium static equation: $F_B^e = F_B^{SMA}$ (30)

Mounting equation: $f_B^e + f_B^{SMA} = \Delta L_0$ (31)

where K^e is the stiffness of the elastic spring. The resolution of this four equation system allows us to find the values of the four quantities f_B^e, f_B^{SMA}, F_B^e and F_B^{SMA}. Figure 18 gives the graphical solution of the previous system of equations.

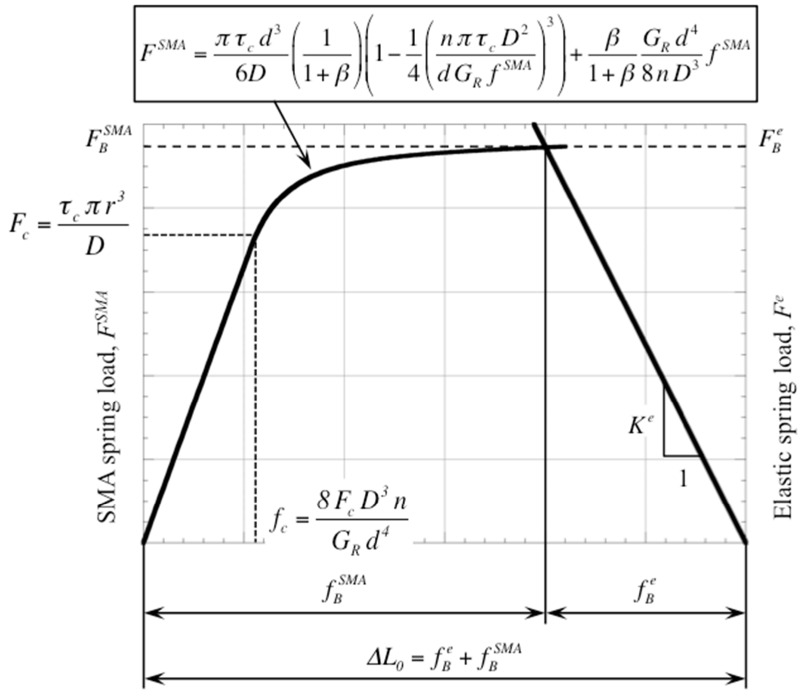

Fig. 18. Graphical determination of the initial position (B) of the SMA linear bias-elastic spring actuator.

Now that the initial state of the SMA spring actuator is known, the procedure to determine the evolution of the actuator during an actuation stage will be described in the following. This procedure is based on the model describing the thermo-mechanical behavior of a stress-assisted two-way R-phase SMA helical spring proposed in Section §3 (Eqns (22), (23) and (27)). Knowing the temperature, T, and its rate, $\dot{T}$, it is necessary to proceed using the three following steps:

Step 1: select the hysteresis loop branch according to the temperature variation sign (Fig. 11)

$$\text{if } \dot{T} > 0,\ z_s(T,f) = w \cdot \psi_1\left(T, \frac{8D}{\pi d^3} K_e (\Delta L_0 - f)\right) + w \tag{32}$$

$$\text{if } \dot{T} \leq 0,\ z_s(T,f) = (1-v) \cdot \psi_2\left(T, \frac{8D}{\pi d^3} K_e (\Delta L_0 - f)\right) + v \tag{33}$$

Step 2: solve Newton's law equation in quasi-static conditions, using a numerical procedure, enabling the determination of the deflection f

$$\frac{K_e \cdot (\Delta L_0 - f)}{K_a \cdot (1 - z_s(T,f)) + K_R \cdot z_s(T,f)} + \frac{\pi n D^2}{d} \cdot \left(\mu^{tr} - a \cdot (T - T_{ref})\right) \cdot z_s(T,f) - f = 0 \qquad (34)$$

Step 3: update the memory variables, v and w, using the f calculated in Step 2

$$\text{if } \dot{T} > 0, \quad \begin{cases} \dot{w} = 0 \\ v = \dfrac{z_s(T,f) - \psi_2\left(T, \dfrac{8D}{\pi d^3} \cdot K_e \cdot (\Delta L_0 - f)\right)}{\left(1 - \psi_2\left(T, \dfrac{8D}{\pi d^3}\right)\right)} \end{cases} \qquad (35)$$

$$\text{if } \dot{T} \leq 0, \quad \begin{cases} w = \dfrac{z_s(T,f)}{1 + \psi_1\left(T, \dfrac{8D}{\pi d^3} \cdot K_e \cdot (\Delta L_0 - f)\right)} \\ \dot{v} = 0 \end{cases} \qquad (36)$$

Let us introduce the relative displacement of the mobile part, y, defined by the following equation:

$$y = f_D - f \qquad (37)$$

where f and f_D are the current deflection and the deflection at position (D) of the SMA spring, respectively. f_D is given by the resolution of the following equation:

$$\frac{K_e \cdot (\Delta L_0 - f_D)}{K_a \cdot (1 - z_s(T_D, f_D)) + K_R \cdot z_s(T_D, f_D)} + \frac{\pi n D^2}{d}\left(\mu^{tr} - a.(T_D - T_{ref})\right).z_s(T_D, f_D) - f_D = 0 \qquad (38)$$

where T_D is the temperature at the position (D) and $z_s(T_D, f_D)$ is given by:

$$z_s(T_D, f_D) = \Psi_1\left(T_D, \frac{8D}{\pi d^3} \cdot K_e \cdot (\Delta L_0 - f_D)\right) + 1 \qquad (39)$$

This set of equations permits the description of the thermo-mechanical behavior of an SMA linear bias-elastic spring actuator taking into account the internal loop phenomena.

4.3. Experimental validation of the simplified thermo-mechanical model for the SMA linear bias-elastic spring actuator

The previous thermo-mechanical model for the SMA linear bias-elastic spring actuator was confronted with experimental results. To achieve this, an SMA linear bias-elastic spring actuator was developed (Fig. 19).

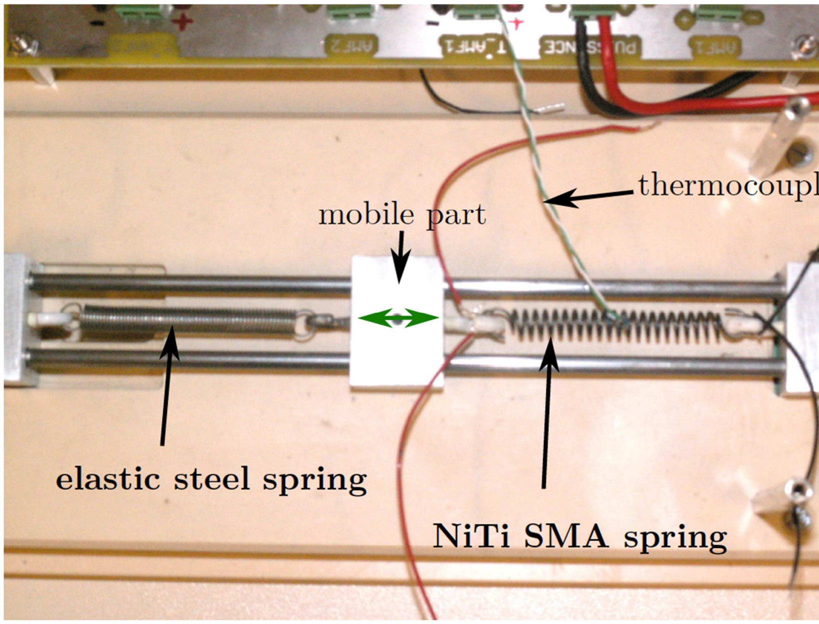

Fig. 19. Top view of the SMA linear bias-elastic spring actuator developed.

The actuator developed was composed of two traction springs mounted in series. The first (on the left in Fig. 19) was an elastic steel spring of stiffness K_e = 0.09 N/mm. The second spring (on the right in Fig. 19) was an *R*-phase NiTi spring with the same geometric and material characteristics as those used in Sections 2.4 and 3.4.

To ensure temperature homogeneity, heating and cooling loadings were performed using the same thermal chamber as before. The position of the mobile part, *y*, was measured by a laser sensor with a resolution of about 50 µm. The SMA spring temperature was measured using a K-type thermocouple (Fig. 19). Two cooling and heating cycles, between 60°C and 25°C, were performed with two different prestrain values (*i.e.*, ΔL_0 = 40 mm and ΔL_0 = 50 mm). Figure 20 shows the comparisons between experimental and numerical results. It can be observed that the numerical forecasts were good and that the proposed model was able to predict the actuator behavior with good accuracy.

- a - - b -

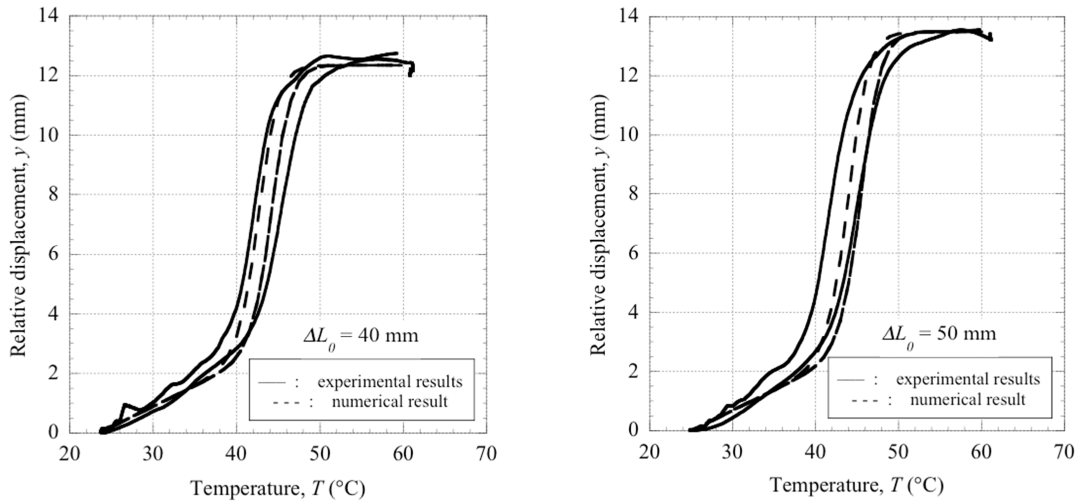

Fig. 20. Comparison between experimental and numerical results concerning the thermo-mechanical behavior of an SMA linear bias-elastic spring actuator:

- a - Prestrain value, ΔL_0 = 40 mm,

- b - Prestrain value, ΔL_0 = 50 mm.

5. Conclusion

This contribution analyses the quasi-static thermo-mechanical behavior of SMA helical spring-based actuators. In a primary step, analytical or pseudo-analytical tools have been proposed to describe both pseudo-plastic and stress assisted two-way memory effect behaviors of SMA helical springs. Particular attention has been paid to *R*-phase SMA helical spring-based actuators (*i.e.*, springs made in NiTi and concerned by *R*-phase transformation phenomenon). The proposed simplified models (*i.e.*, based on beam theory framework) have been validated using experimental results obtained as a part of this work. In a second step, a thermo-mechanical constitutive model for linear bias-spring actuators has been proposed. An SMA linear bias-elastic spring actuator has been developed and used to study the relevance of the proposed model. Numerical simulations are in good agreement with experimental data. All the models proposed in this work can be used for the design of linear-actuators using *R*-phase SMA helical springs.

References

[1] D. C. Lagoudas (ed.), Shape Memory Alloys: Modeling and Engineering Applications. Springer US, 2008.

[2] H.C. Kim, Y.I. Yoo and J.J. Lee, Development of a niti actuator using a two-way shape memory effect induced by compressive loading cycles. *Sensors and Actuators A: Physical*, 148 (2008) 437–442.

[3] G. Costanza, M.E. Tata, C. Calisti, Nitinol one-way shape memory springs: Thermomechanical characterization and actuator design. *Sensors and Actuators A: Physical*, 157 (2010) 113–117.

[4] J.M. Jani, M. Leary, A. Subic and M.A. Gibson, A review of shape memory alloy research, applications and opportunities. *Materials & Design*, 56 (2014) 1078–1113.

[5] M.A. Zainal, S. Sahlan and M.S.M. Ali, Micromachined shape-memory-alloy microactuators and their application in biomedical devices. *Micromachines*, 6 (2015) 879.

[6] B. Holschuh, E. Obropta and D. Newman, Low spring index niti coil actuators for use in active compression garments. IEEE/ASME *Transactions on Mechatronic*, 20 (2015) 1264–1277.

[7] M. Sreekanth, A. Mathew and R. Vijayakumar, Modeling and control of SMA helical spring actuated unconventional locomotion systems. In: Proceedings of 2015 IEEE International Conference on Power, Instrumentation, Control and Computing. 1–4, 2015.

[8] H. Rodriguea, W. Wanga, M.W. Hana, Y.J. Quana, S.H. Ahn, Comparison of mold designs for SMA-based twisting soft actuator. *Sensors and Actuators A: Physical*, 237 (2016) 96–106.

[9] K. Ikuta, Micro/miniature shape memory alloy actuator. In: Proc. IEEE International Conference on Robotics and Automation. 2156–2161, 1990.

[10] A. Nespoli, S. Besseghini, S. Pittaccio, E. Villa, S. Viscuso, The high potential of shape memory alloys in developing miniature mechanical devices: A review on shape memory alloy mini-actuators. *Sensors and Actuators A: Physical*, 158 (2010) 149–160.

[11] J.M. Jani, M. Leary and A. Subic, Designing shape memory alloy linear actuators: A review. *Journal of Intelligent Material Systems and Structures*, 28 (2017) 1699–1718.

[12] H. Yuan, J.C. Fauroux, F. Chapelle and X. Balandraud, A review of rotary actuators based on shape memory alloys. Accepted in *Journal of Intelligent Material Systems and Structures*, (2017).

[13] K. Otsuka, C.M. Wayman, Shape Memory Materials, Cambridge University Press, 1999.

[14] K. Wada and Y. Liu, On the mechanisms of two-way memory effect and stress-assisted two-way memory effect in NiTi shape memory alloy. *Journal of Alloys and Compounds*, 449 (2008) 125–128.

[15] N. Nikdel and M. Badamchizadeh, Design and implementation of neural controllers for shape memory alloy-actuated manipulator. *Journal of Intelligent Material Systems and Structures*, 26 (2015) 20–28.

[16] A. Ianagui and E.A. Tannuri, A sliding mode torque and position controller for an antagonistic SMA actuator. *Mechatronics*, 30 (2015) 126–139.

[17] R. Romano and E.A. Tannuri, Modeling, control and experimental validation of a novel actuator based on shape memory alloys. *Mechatronics*, 19 (2009) 1169–1177.

[18] G. Costanza, M. Tata and C. Calisti, Nitinol one-way shape memory springs: Thermomechanical characterization and actuator design. *Sensors and Actuators A: Physical*, 157 (2010) 113–117.

[19] B. Holschuh, E. Obropta and D. Newman, Low spring index niti coil actuators for use in active compression garments. IEEE/ASME *Transactions on Mechatronics*, 20 (2015) 1264–1277.

[20] M.A. Savi, P.M.C.L. Pacheco, M.S. Garcia, R.A.A. Aguiar, L.F.G. de Souza and R.B. da Hora, Nonlinear geometric influence on the mechanical behavior of shape memory alloy helical springs. *Smart Materials and Structures*, 24 (2015) 035012.

[21] P. Šittner, M. Landa, P. Lukàs and V. Novàk, R-phase transformation phenomena in thermomechanically loaded NiTi polycrystals. *Mechanics of materials*, 38 (2006) 475–492.

[22] P. Šittner, P. Sedlák, M. Landa, V. Novàk and P. Lukàs, *In situ* experimental evidence on R-phase related deformation processes in activated NiTi wires. *Materials Science and Engineering A*, 438–440 (2006) 579–584.

[23] G. Helbert, L. Saint-Sulpice, S. Arbab Chirani, L. Dieng, T. Lecompte, S. Calloch and P. Pilvin, Experimental characterisation of three-phase NiTi wires under tension. *Mechanics of Materials*, 79 (2014) 85–101.

[24] Y. Toi, J.B. Lee and M. Taya, Finite element analysis of superelastic, large deformation behavior of shape memory alloy helical springs. *Computers and Structures*, 82 (2004) 1685-1693.

[25] G. Attanasi, F. Auricchio and M. Urbano, Theoretical and Experimental Investigation on SMA Superelastic Springs. *Journal of Materials Engineering and Performance*, 20 (2011) 706–711.

[26] L. Saint-Sulpice, S. Arbab Chirani and S. Calloch, Thermomechanical cyclic behavior modeling of Cu-Al-Be SMA materials and structures, *International Journal of Solids and Structures*, 49 (2012) 1088-1102.

[27] A.F. Saleeb, B. Dhakal, M.S. Hosseini and S.A. Padula Ii, Large scale simulation of NiTi helical spring actuators under repeated thermomechanical cycles. *Smart Materials and Structures*, 22 (2013) 094006.

[28] P. Sedlák, M. Frost, A. Kruisová, K. Hi□manová, L. Heller and P. Šittner, Simulations of mechanical response of superelastic NiTi helical spring and its relation to fatigue resistance. *Journal of Materials Engineering and Performance*, 23 (2014) 2591-2598.

[29] M.A. Savi, P.M.C.L. Pacheco, M.S. Garcia, R.A.A. Aguiar, L.F.G. De Souza and R.B. Da Hora, Nonlinear geometric influence on the mechanical behavior of shape memory alloy helical springs. *Smart Materials and Structures*, 24 (2015) 035012.

[30] M. Frost, P. Sedlák, L. Kade□ávek, L. Heller and P. Šittner, Modeling of mechanical response of NiTi shape memory alloy subjected to

combined thermal and non-proportional mechanical loading: A case study on helical spring actuator. *Journal of Intelligent Material Systems and Structures*, 27 (2016) 1927-1938.

[31] A.R. Damanpack, M. Bodaghi and W.H. Liao, A finite-strain constitutive model for anisotropic shape memory alloys. *Mechanics of Materials*, 112 (2017) 129-142.

[32] J. Wang, Z. Moumni, W. Zhang and W. Zaki, A thermomechanically coupled finite deformation constitutive model for shape memory alloys based on Hencky strain. *International Journal of Engineering Science*, 117 (2017) 51-77.

[33] H. Tobushi and K. Tanaka, Deformation of a shape memory alloy helical spring. (Analysis based on stress-strain-temperature relation). *JSME International Journal*, Series 1: Solid Mechanics, Strength of Materials, 34 (1991) 83-89.

[34] R.A.A. Aguiar, M.A. Savi and P.M.C.L. Pacheco, Experimental and numerical investigations of shape memory alloy helical springs. *Smart Materials and Structures*, 19 (2010) 025008.

[35] R. Mirzaeifar, R. Desroches and A. Yavari, Exact solutions for pure torsion of shape memory alloy circular bars. *Mechanics of Materials*, 42 (2010) 797-806.

[36] I. Spinella, E. Dragoni and F. Stortiero, Modeling, prototyping, and testing of helical shape memory compression springs with hollow cross section. *Journal of Mechanical Design*, Transactions of the ASME, 132 (2010) 0610081-0610089.

[37] I. Spinella and E. Dragoni, Analysis and Design of Hollow Helical Springs for Shape Memory Actuators. *Journal of Intelligent Material Systems and Structures*, 21 (2010) 185-199.

[38] R. Mirzaeifar, R. Desroches and A. Yavari, A combined analytical, numerical, and experimental study of shape-memory-alloy helical springs. *International Journal of Solids and Structures*, 48 (2011) 611-624.

[39] R.A.A. de Aguiar, W.C. de Castro Leão Neto, M.A. Savi, and P.M. Calas Lopes Pacheco, Shape memory alloy helical springs performance: Modeling and experimental analysis. *Materials Science Forum*, 758 (2013) 147-156.

[40] B. Huang, W. Pu, H. Zhang, H. Wang and G. Song, A phenomenological model for superelastic shape memory alloy helical springs. *Advances in Structural Engineering*, 18, (2015) 1345-1354.

[41] S. Enemark, I.F. Santos and M.A. Savi, Modelling, characterisation and uncertainties of stabilised pseudoelastic shape memory alloy helical springs. *Journal of Intelligent Material Systems and Structures*, 27 (2016) 2721-2743.

[42] B. Heidari, M. Kadkhodaei, M. Barati and F. Karimzadeh, Fabrication and modeling of shape memory alloy springs. *Smart Materials and Structures*, 25 (2016) 125003.

[43] A. Barré de Saint-Venant, Mémoire sur la torsion des prismes à base rectangle et à base losange, et sur une petite correction numérique à faire subir, en général, aux moments de torsion, Comptes Rendus hebdomadaires des séances de l'Académie des Sciences, 17 (1843).

[44] S. Timoshenko, Strength of Materials: Elementary Theory and Problems, volume 1. CBS Publishers and Distributors, 1956.

[45] K. Taillard, S. Arbab Chirani, S. Calloch and C. Lexcellent, Equivalent transformation strain and its relation with martensite volume fraction for isotropic and anisotropic shape memory alloys. *Mechanics of Materials*, 40 (2008) 151–170.

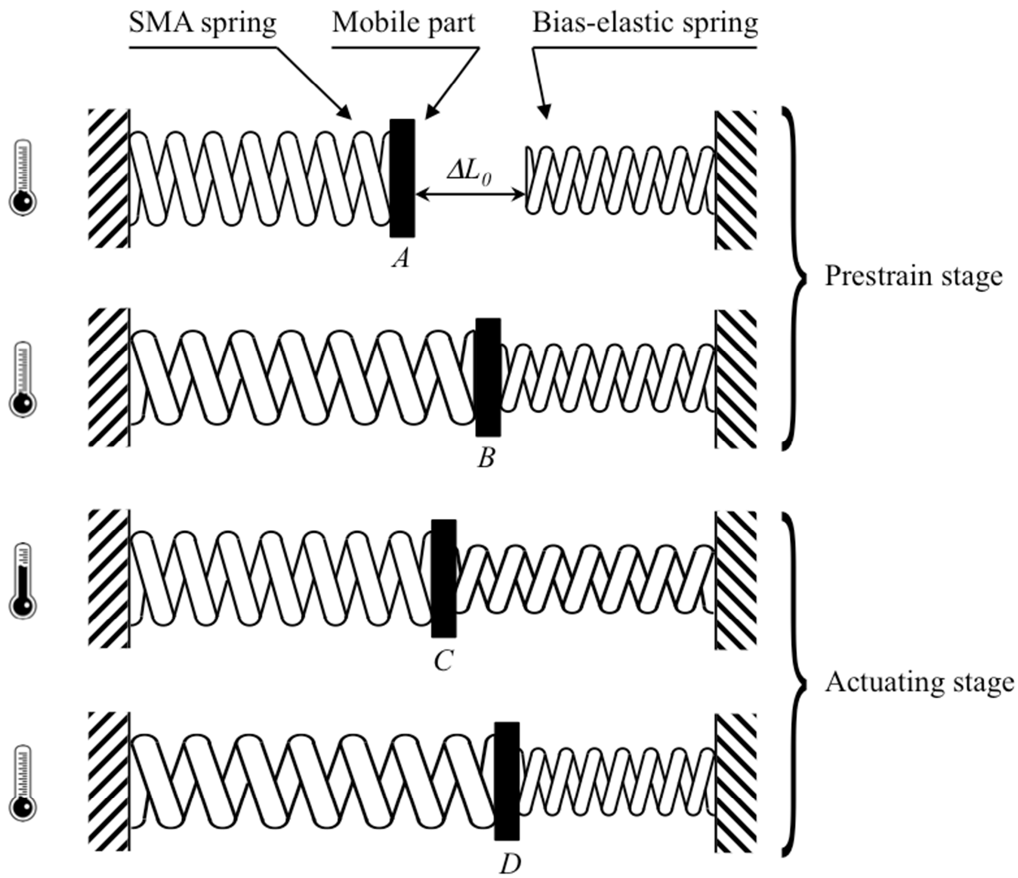

Schematic representation of the two stages in the operation of an SMA linear bias-elastic spring actuator.